Studies of the photonic and optical-frequency phonon properties of arrays of selectively grown GaN micropyramids

D. Coquillat,[1,a)] M. Le Vassor d'Yerville,[1] M. Kazan,[1] C. Liu,[2] I. M. Watson,[2] P. R. Edwards,[3] R. W. Martin,[3] H. M. H. Chong,[4] and R. M. De La Rue[4]
[1]*Groupe d'Etude des Semiconducteurs, UMR 5650 CNRS-UM2, Place E. Bataillon, 34095 Montpellier, France*
[2]*Institute of Photonics, SUPA, University of Strathclyde, 106 Rottenrow, Glasgow G4 0NW, United Kingdom*
[3]*Department of Physics, SUPA, University of Strathclyde, 107 Rottenrow, Glasgow G4 0NG, United Kingdom*
[4]*Optoelectronics Research Group, Department of Electronics and Electrical Engineering, Glasgow University, Glasgow G12 8LT, United Kingdom*

(Received 2 November 2007; accepted 7 December 2007; published online 28 February 2008)

An array of GaN micropyramids containing a near-surface $In_xGa_{1-x}N/GaN$ single quantum well has been fabricated using selective area epitaxial overgrowth above a patterned silica mask. The pyramid array has been studied by means of angle-resolved reflection measurements using *s*- and *p*-polarized incident light in the near- and mid-infrared optical ranges. We have found that the periodic array of flat-topped pyramids shows marked resonances in the near-infrared optical range due to resonant Bloch modes within the extraction cone and that the angular dispersion of these modes exhibits strong photonic crystal characteristics. The experimental results are in good agreement with the photonic band structure calculated using a scattering matrix formalism. The mid-infrared optical anisotropy properties of the micropyramids were investigated to probe the infrared active phonons of the pyramid array. The A_1(LO) phonon of the $In_xGa_{1-x}N/GaN$ single quantum well was identified and the InN mole fraction was estimated from the mode behavior.
 [DOI: 10.1063/1.2841722]

I. INTRODUCTION

Group III-nitride semiconductors are now heavily used in the production of blue light emitting diodes (LEDs), and a variety of attempts are focusing on improving the light extraction efficiency by different technologies. Examples of these technologies include photonic crystal slabs, hexagonal pyramid shaped LEDs,[1] and a roughened extraction surface featuring a high density of truncated hexagonal pyramids.[2] Photonic crystal slabs offer various degrees of freedom for improving the extraction efficiency[3–6] and controlling the direction of emission.[7] Planar photonic crystal slabs support different kinds of electromagnetic bound modes that are usually classified into two categories: guided and resonant Bloch modes. In-plane guided modes located below the cladding light line in the dispersion diagram are completely confined in the slab, without any coupling to external radiation. Resonantly coupled Bloch modes lying above the light line appear as resonances within the continuum of radiative modes. They can couple to external radiation and provide an excellent way of extracting the light from within a LED structure.[8]

The previous work on group III-nitride photonic crystals has focused essentially on photonic crystal slabs with patterned lattices of holes etched through the III-nitride layers.[3–7,9–11] In contrast, the present paper considers a selectively grown photonic crystal slab consisting of a two-dimensional array of hexagonal-base GaN pyramids that also contain an $In_xGa_{1-x}N/GaN$ single quantum well (SQW), in contact with a thick seed GaN layer. The selective area growth (SAG) approach to the fabrication of III-nitride photonic crystals can potentially provide more efficient and long-lived light emitters due to the elimination of damage effects produced by direct etching processes in the active layers. Moreover, it potentially can produce efficient microcavities due to smoother facet walls.

The dispersion of resonant Bloch modes in a photonic crystal can be measured by surface coupling reflectivity measurements at variable incidence and azimuthal angles. The coupling between the incoming wave and photonic modes gives rise to resonant features for which the evolution as a function of the incident and azimuthal angles leads to the determination of the photonic band dispersion.

In this work we present the results of both experimental and theoretical investigations of the band structure of a two-dimensional array of GaN pyramids formed by SAG. We have examined the dispersion characteristics of the resonant Bloch modes, although this behavior was observed only at much longer wavelengths than the blue/UV part of the visible spectrum, which is ultimately the region of greatest interest. Toward this end, we have collected angularly resolved reflection spectra in the *near*-infrared (IR) spectral regions where the lowest resonances appear. We have found that, in a periodic array of flat-topped pyramids, marked resonances are observable within the extraction cone and that the angular dispersion of the photons exhibits strong photonic crystal characteristics. In addition, *mid*-IR angularly resolved spectrometry is an attractive and powerful tool for the optical characterization of semiconductor thin films. The lattice vi-

a)Electronic mail: dominique.coquillat@univ-montp2.fr.

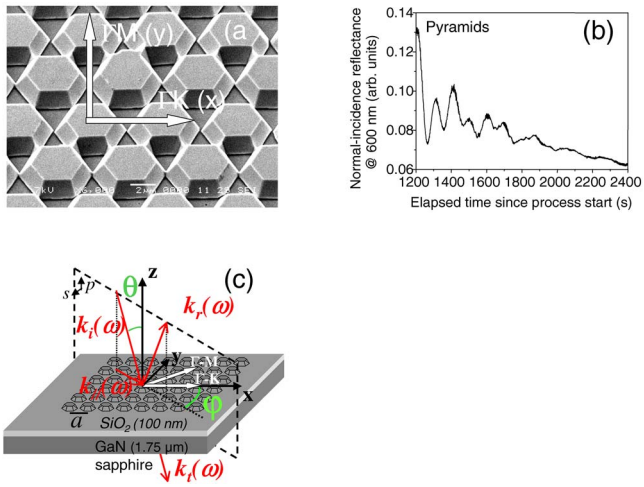

FIG. 1. (Color online) (a) Scanning electron micrograph of the selectively grown array with an in-plane period a of 5.75 μm. The six $\{10\bar{1}1\}$ sloping side facets and the {0001} top facets of the pyramids result from the growth habit of the epitaxial material—and the final shape is controlled by terminating the growth at the desired time. (b) *In situ* measurement of the optical reflectance from a pyramid array, taken at normal incidence at a wavelength of 600 nm during the high-temperature GaN growth and showing rich oscillatory structure, indicative of smooth (0001) facets forming from the start of growth. (c) Schematic representation of the experimental configuration. θ and φ are, respectively, the incident and azimuthal angles. $k(\omega)$ is the wave vector of the incident beam and $k_{\parallel}(\omega)$ is the in-plane component. ΓK and ΓM are the symmetry directions of the Brillouin zone of the photonic crystal and correspond to $\varphi=0°$ and $\varphi=30°$, respectively.

bration properties of the array of pyramids have been investigated using reflection spectra and by rotating the sample. The *s*- and *p*-polarized incident light were used in order to predominantly identify the IR-active A_1(LO) phonon behavior of the $In_xGa_{1-x}N/GaN$ SQW grown on the pyramidal facets, and information on the $In_xGa_{1-x}N$ alloy composition has been extracted from the phonon mode parameters.[12]

II. SAMPLE GROWTH AND OTHER EXPERIMENTAL DETAILS

Arrays of hexagonal pyramids displaying either sharp tips or flat-topped forms, and containing one or more near-surface $In_xGa_{1-x}N/GaN$ quantum wells, have been produced using SAG through micrometer-scale windows in silica (SiO_2) mask layers.[13] The present paper describes measurements only on a flat-topped structure, as illustrated in the scanning electron microscope (SEM) image in Fig. 1(a). A 1.75 μm thick (0001) oriented GaN-on-sapphire seed layer was first covered with a 100 nm thick SiO_2 mask layer, deposited by plasma-enhanced chemical vapor deposition (PECVD). This mask layer was then patterned by conventional lithography and wet etching to form a triangular array of circular windows of radius of 2.5 μm with a period of 5.75 μm. The seed wafer was covered with 15 separate patterned fields, each ~5 mm square. The parameters of the second epitaxial step, performed at a setpoint temperature (ST) of 1100 °C, have been optimized to grow hexagonal-based pyramidal structures, with side facets formed by $\{10\bar{1}1\}$ planes—and with top facet formed by the {0001} plane. *In situ* measurements of the optical reflectance, taken at normal incidence at wavelengths of 450, 600, and 800 nm, gave a strong suggestion that the pyramids developed with optically smooth top facets throughout their growth [Fig. 1(b)]. This is in agreement with time-sequence SEM images reported by Miyake *et al.* for certain growth conditions,[14] although Jetter *et al.* observed initially rough surfaces by SEM for growth conditions nominally similar to our own.[15] *In situ* reflectometry has been applied only rarely to the growth of three-dimensional GaN structures, but data from such growths can be understood if the interplay between Fabry–Perot multilayer interference and reflections from a stepped surface is considered.[16] Each pyramidal structure contained an $In_xGa_{1-x}N/GaN$ SQW, deposited near the end of the growth sequence at a ST of 800 °C, and capped with a 6 nm layer of GaN grown at the same temperature. During overgrowth of the pyramids, these SQWs formed both on the top facet and inclined sidewalls. The $In_xGa_{1-x}N$ growth conditions were chosen to give a nominal 2.5 nm well thickness on a standard planar GaN (0001) buffer layer, and cathodoluminescence (CL) measurements made on a macroscopic reference window in the SiO_2 mask confirmed a SQW peak emission wavelength of ~470 nm. To further investigate whether the additional features observed in the mid-IR optical-frequency range came from near-surface material (grown at relatively low temperatures), we have examined three model epistructures: (i) a planar epilayer of high-temperature GaN (HT-GaN), representative of the "bulk" pyramid material and the GaN seed layer underneath the pyramids, grown at a ST of 1140 °C; (ii) a 200 nm thick $In_xGa_{1-x}N$ epilayer grown at a ST of 820 °C with an InN fraction measured by Rutherford backscattering spectrometry (RBS) of ~11.5%, representative of the SQW grown over the pyramids; and (iii) a structure terminated with a ~200 nm thick layer of low-temperature GaN, grown at a ST of 830 °C, and representative of the SQW cap layer. All these samples were grown on (0001)-oriented sapphire substrates, and more detail on the growth conditions is reported in Ref. 17. The last two structures have buffer layers of HT-GaN below the topmost layers of principal interest.

We have used atomic force microscopy to investigate the shape of the pyramids and to obtain information about the period and vertically dependent GaN filling factor of the photonic crystal structure. The crystallographic axes along x and y (perpendicular to the c-axis of GaN) and the high symmetry directions ΓK and ΓM of the pyramid array are almost exactly aligned [Fig. 1(a)]. The uniform hexagonal pyramids were 1.30 μm in height—and the lengths of each side of the top facet and of the base were 2.02 and 2.88 μm, respectively. The size of the pyramids was homogenous for most of the 5 mm square area examined.

Near- and mid-IR angularly resolved reflection spectra were recorded with a Fourier-transform infrared spectrometer in the wave-number range between 370 and 3000 cm^{-1} (3.3–27 μm), with a spectral resolution of 2 cm^{-1}. The polarization of the weakly focused incident light was selected to be either perpendicular (s) or parallel (p) to the plane of incidence by means of a Cambridge Physical Sciences IGP 225 polarizer [Fig. 1(c)]. The IR probe beam spot size at the sample surface was approximately 1 mm^2 at normal incidence. Using small progressive changes of the azimuthal

angle φ of the pyramid array between 0° and 60° and multiple angles of incidence θ between 6° and 60°, we have observed the dispersion of the resonant Bloch modes of the pyramid array, and the evolution of the LO phonon modes of GaN and of the $In_xGa_{1-x}N/GaN$ SQW. From this information, the photonic band dispersion of the photonic structure was reconstructed and the InN content of the $In_xGa_{1-x}N/GaN$ SQW was determined. Details of the angularly resolved experiments used here are described in Ref. 18. Micro-Raman measurements were performed on the top facet of an individual pyramid using the 488 and 647.1 nm excitation lines from an argon-krypton laser, in a backscattering geometry. The spot size was about 2 μm and the sample was excited along the (0001) direction. It should be noted that the $In_xGa_{1-x}N/GaN$ SQW layer was too thin for it to be possible to detect phonons in $In_xGa_{1-x}N$ by Raman spectroscopy. All the measurements were performed at room temperature.

The experimentally determined photonic band structure was compared with theoretical results obtained with a scattering matrix method.[19,20] In this scattering matrix formalism, the vertical profile of the finite height two-dimensional photonic crystal structure is considered as a stack of layers with a vertically invariant dielectric distribution. The multilayer structure is bound between a semi-infinite substrate (sapphire), below, and the semi-infinite ambient, above. No periodic or absorbing boundary conditions are then introduced along the vertical direction, which allows an accurate three-dimensional description of the structure to be computed. The in-plane periodicity of the SiO_2 and pyramid layers is taken into account by an in-plane Bloch description of the electromagnetic field. The vertical shape of the pyramids was modeled by stacking up three layers consisting of triangular lattices of GaN hexagonal pillars. The gradual addition of these steps with a constant average filling factor showed that the nonverticality of the pyramidal facets does not drastically modify the shape of the band structure. In the calculation the refractive indices have been fixed as $n_{\text{sapphire}}=1.58$ and $n_{\text{GaN}}=2.32$.

III. EXPERIMENTAL AND THEORETICAL PHOTONIC BAND STRUCTURE OF THE RESONANT BLOCH MODES IN THE NEAR-IR OPTICAL RANGE

Figure 2 presents the typical near-IR reflection spectra, in the transparent region of the sample (1000–3000 cm^{-1}), for *s*- and *p*-polarized light, obtained for two angles of incidence (θ=9° and 60°) along the ΓM symmetry orientation. The spectra are characterized by relatively sharp resonance features arising from the excitation of the resonant Bloch modes. The resonances in the reflection spectra for 60° angle of incidence reach relative amplitudes as large as 0.30. Extracting the frequencies of the most significant resonances as a function of the in-plane wave-vector values along ΓK and ΓM results in the dispersions illustrated in Figs. 3(a) and 3(b) for *s*- and *p*-polarized incident light, respectively. Good agreement is found when comparing the photonic bands extracted from experimental data with theoretical values. As a first remark, we note that the calculated photonic band structure reproduces all the important resonances of the experiment—and also the global shift of the resonances with angle of incidence. The discrepancies can be attributed to several factors. Firstly, the frequency dispersions of the GaN and sapphire dielectric functions, which are not introduced in the calculations, are rather large in the range of wavelengths investigated in the experiments. In addition, various predicted parameters of the structure may not fit exactly the experimental ones, such as the thicknesses of the layers or the averaged filling factor of the pyramid layer. However, the good agreement between the experimental and calculated band structures suffices to account for the experimentally demonstrated photonic crystal dispersion phenomena.

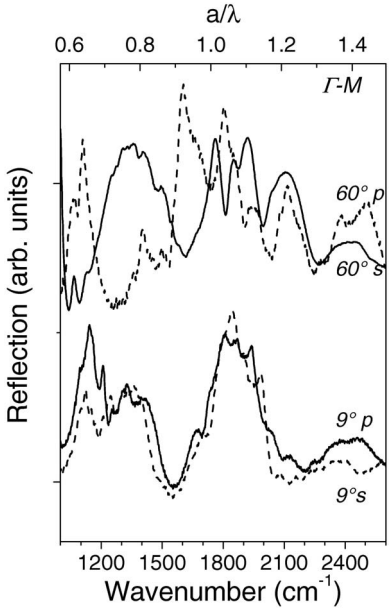

FIG. 2. Typical near-IR reflection spectra of the selectively grown pyramid array, along the ΓM symmetry orientation, for two angles of incidence (9° and 60°) and for *s*- and *p*-polarization.

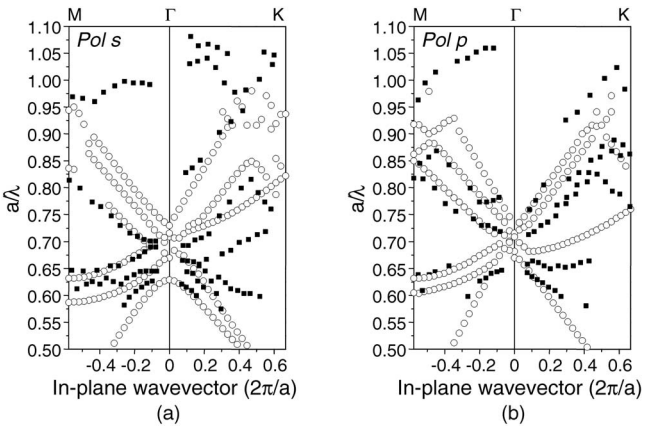

FIG. 3. Measured dispersion of the photonic bands as derived from the resonances in the reflection spectra (■) compared with calculated dispersion (○) for (a) *s*-polarized incident light and (b) *p*-polarized incident light. The shape of the pyramids was modeled by stacking up three layers consisting of a triangular lattice of GaN hexagonal pillars. The three layers have the same thickness but different values of the GaN filling factors (f_{GaN}=75%, 54.5%, and 37.0% from the bottom to the top of the pyramids).

IV. PHONONS IN GaN PYRAMIDS CONTAINING AN $In_xGa_{1-x}N$ SQW AND PHOTONIC FEATURES IN THE MID-IR OPTICAL RANGE

Mid-IR reflectivity is an efficient technique for investigation of the vibrational properties of group III-nitrides and especially for the extraction of alloy composition in very thin layers by the determination of the phonon frequencies. We have used this technique to determine the alloy composition of the $In_xGa_{1-x}N/GaN$ SQW grown on the facets of the pyramids. As shown by experimental studies and theoretical predictions,[12,21,22] the $E_1(TO)$ and $A_1(LO)$ phonons in $In_xGa_{1-x}N$ exhibit a one-mode behavior for the full composition range. In these alloys, the $A_1(LO)$ phonon frequencies shift approximately linearly toward lower frequencies with increasing x, in a range between the limiting phonon frequencies of the two binary crystals—and the influence of possible strain effects is negligible.[12] Recently, Hu *et al.*[23] explored the optical anisotropy and Berreman's effects on the IR reflectivity of GaN and $Ga_{1-x}Mn_xN$ epilayers. They concluded that the dip observed for p-polarized incident light, in the range of 735–755 cm^{-1} when the angle of incidence increases from 0° up to 70°, is due to the optical anisotropy, i.e., the $A_1(LO)$ phonon mode rather than the $E_1(LO)$ mode. They have also shown that in the thin samples the $A_1(LO)$ mode was not sensitive to Berreman's effect. In order to determine the alloy composition of the $In_xGa_{1-x}N/GaN$ SQWs, we have probed the IR-active phonons of the pyramid array—and of samples representative of the component layers of the pyramid samples—and we have used the database established by Kasic *et al.*[12] and the conclusions of Hu *et al.*[23] to extract the InN fraction in the SQW from the IR-active $A_1(LO)$ phonon frequency of the alloy.

Figure 4 shows the experimental mid-IR reflection spectra of the four epilayers: (i) the pyramid array, (ii) the HT-GaN seed layer, (iii) the thick $In_xGa_{1-x}N$ epilayer, and (iv) the thick low-temperature GaN epilayer (representative of the SQW cap)—over the range of 370–1000 cm^{-1}—measured at near-normal incidence ($\theta \sim 10°$) with the propagation vector being almost parallel to the c-axis and using unpolarized light. This wave-number range is located in the overlapping reststrahlen regions of the sapphire and of GaN, where the reflection is high. For all four samples, the measured mid-IR response is influenced by distinct features due to the sapphire substrate (marked by an asterisk), which, in part, coincide with the GaN phonon modes. For example, the broadening edge at 910 cm^{-1} is assigned to the reststrahlen band of the sapphire substrate. The $A_1(LO)$ phonon shows a minimum dip in reflection. Due to optical anisotropy, the $A_1(LO)$ phonon mode is forbidden at the normal incidence, but the dip began to develop at small angles.[23,24] The position of the dip at about 735 cm^{-1}, for $\theta \sim 10°$ and for each of the four samples, agrees well with the position of the peak attributed to the $A_1(LO)$ phonon mode of GaN in the micro-Raman experiments (Fig. 5). In the case of the thick $In_xGa_{1-x}N$ epilayer (see Fig. 4), the spectrum exhibits a feature with a minimum around 713 cm^{-1} that is associated with the $A_1(LO)$ photon mode of the alloy. According to the composition dependence of the $In_xGa_{1-x}N$ $A_1(LO)$ phonon mode frequency,[12] and neglecting possible strain effects, the value deduced for the InN fraction is ~14%. This value is reasonably consistent with the composition measured by RBS. The spectrum from the GaN epilayer grown at a low temperature reveals a weak feature at 699 cm^{-1}, which may originate from defects. The IR spectrum of the pyramid array in Fig. 4 exhibits a larger number of features, of which the dip at 720 cm^{-1} is assigned to the $A_1(LO)$ mode of the $In_xGa_{1-x}N/GaN$ SQW (720 cm^{-1})—as we shall see in the following—and the feature at 699 cm^{-1} may be assigned to the cap layer. A somewhat surprising result is the presence of additional features (AFs) in the frequency range of 550–775 cm^{-1}, among which are features at ω_{AF1} = 717 cm^{-1}, ω_{AF3} = 667 cm^{-1}, and ω_{SiO_2} = 612 cm^{-1}. The two other additional features, AF2 and AF4, are not visible in this spectrum. To clarify the origin of all these features, we have focused our analysis on their wave-number position and on their extinction or continued presence, which will determine the sensitivity, or lack thereof, to the values of θ and φ—and to the polarization. The variable-angle reflection spectra of the unpatterned GaN seed layer have also been measured, for comparison. In addition, we have investigated the presence of the additional features in the micro-Raman spectra.

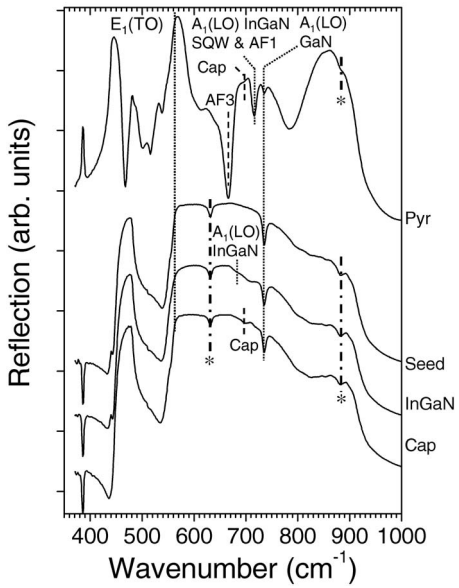

FIG. 4. Mid-IR reflection spectra (θ=10°) for (i) selectively grown GaN pyramid array containing an $In_xGa_{1-x}N$ SQW (labeled Pyr), for (ii) the HT-GaN layer representative of the "bulk" pyramid material and the seed layer beneath the pyramids (labeled Seed), (iii) for the 200 nm thick $In_xGa_{1-x}N$ layer with an InN fraction of ~11.5%, representative of the SQW grown over the pyramids (labeled InGaN), and for (iv) the ~100 nm layer of low-temperature GaN, representative of the SQW cap layer (labeled Cap). The spectra are measured using unpolarized light. The positions of the $E_1(TO)$ and $A_1(LO)$ phonons of the GaN material are indicated by dotted lines. The features marked by an asterisk (for wave number >500 cm^{-1}) are due to the sapphire substrate.

Figures 6(a) and 6(b) show the experimental mid-IR reflection spectra of the unpatterned HT-GaN seed layer, for s- and p-polarized incident light, respectively, which were measured when the angle of incidence θ was varied from 6.5° to 60°. For the s-polarization [Fig. 6(a)], only the $E_1(TO)$ phonons of GaN are IR-active, according to the fact that the $A_1(LO)$ phonon, which propagates parallel to the c-axis, cannot be excited by incident light perpendicular to the plane of

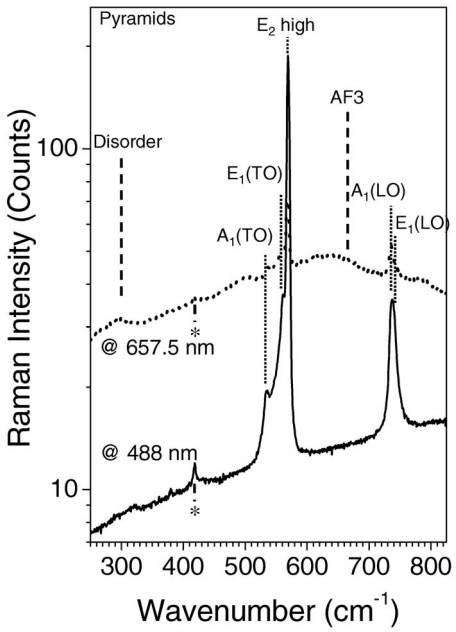

FIG. 5. Micro-Raman spectra acquired from the top facet of a pyramid with the incoming light along the *c*-axis, and with the 488 nm (solid line) and 647.1 nm (dotted line) excitation lines of the laser. The two main peaks at 568 and 735 cm^{-1} are assigned to the E_2(high) and A_1(LO) phonons modes of GaN, respectively. The shoulders at 533 and 560 cm^{-1} are the signature of the forbidden modes A_1(TO) and E_1(TO) of GaN, respectively. The appearance of these forbidden modes is due to the large solid angle of the objective lens of the Raman microscope, a nonstrictly backscattering configuration, and multiple reflections due to the facets of the pyramid. The weak line at 418 cm^{-1} stems from the sapphire substrate. Note that, in the micro-Raman experiments, the SQW is too thin to give detectable phonons in $In_xGa_{1-x}N$.

incidence. The A_1(LO) phonon mode of GaN observed for *p*-polarization becomes progressively stronger when θ increases—and the position of the minimum shifts by more than 19 cm^{-1} in the range of 6.5°–60° [Fig. 6(b)]. This shift is due to optical anisotropy, as discussed by Hu *et al.*[23] The feature at 612 cm^{-1} visible in *p*-polarization was attributed to the SiO_2 film, since this feature disappeared when the SiO_2 was removed by wet etching.

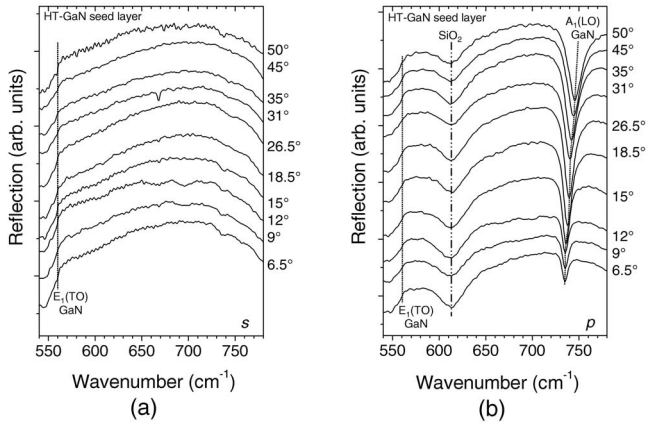

FIG. 6. A series of mid-IR reflection spectra for different values of the angle of incidence θ for the GaN seed layer for (a) *s*-polarization and (b) *p*-polarization. The A_1(LO) mode frequency is very sensitive to the incidence angle. The dashed line showing the angular dispersion of the A_1(LO) mode is provided as a guide to the eye. For convenience, the spectra are shifted vertically.

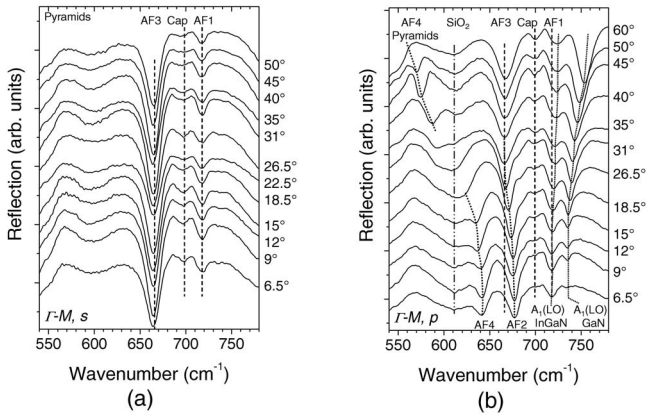

FIG. 7. A series of mid-IR reflection spectra for different values of θ for the pyramid array with the plane of incidence along the ΓM direction and for (a) *s*-polsarization and (b) *p*-polarization. The features labeled A_1(LO)GaN and A_1(LO)InGaN are associated with the A_1(LO) phonon mode of GaN and of the $In_xGa_{1-x}N$ SQW, respectively. The lines showing the angular dispersion of the A_1(LO) modes of GaN and $In_xGa_{1-x}N$/GaN SQW and of the additional features are guides to the eye.

Figures 7(a) and 7(b) represent the reflection spectra of the pyramid array using *s*- and *p*-polarized incident light, respectively, taken along the ΓM orientation. The behavior observed for the A_1(LO) mode of GaN from the pyramids and from the seed layer beneath the pyramids is similar to that of the unpatterned HT-GaN seed layer. Futhermore, in *p*-polarization, a weak feature emerges for small angles of incidence at a frequency around 720 cm^{-1}, on the low-frequency edge of the ω_{AF1} feature, and becomes stronger with increasing angle of incidence. This feature, which is well developed between θ=31° and 60° for *p*-polarization, is absent for *s*-polarization. We have assigned this feature to the A_1(LO) mode of the $In_xGa_{1-x}N$/GaN SQW structure. The A_1(LO) frequency at 720 cm^{-1} for small values of θ corresponds to an alloy composition of x=0.10.[12] CL measurements indicated a peak emission wavelength of ~420 nm from the conformal $In_xGa_{1-x}N$/GaN SQWs grown over the pyramids, and were not able to distinguish the spectra of QWs on the top facets and sloping sidewalls. This emission wavelength is significantly shorter than that observed from the SQW grown on the macroscopic reference area of the unpatterned GaN seed surface (~470 nm). The InN fraction of 0.10 derived from the A_1(LO) frequency characteristics of $In_xGa_{1-x}N$/GaN SQWs in the pyramid zone is in good agreement with the results in Ref. 17, which reports on the composition of a ten-period $In_xGa_{1-x}N$/GaN multiple QW emitting at ~410 nm, grown on a conventional planar (0001)-oriented GaN buffer layer. Note that no $In_xGa_{1-x}N$ phonon modes could be observed in Raman studies of the pyramids (Fig. 5). It should be stated that the reflection spectra for the ΓM orientation are not displayed because they do not carry any extra information on the A_1(LO) phonon mode behavior of the $In_xGa_{1-x}N$/GaN SQW. As shown in Figs. 7(a) and 7(b), the two broad features AF1 and AF3 around 717 and 667 cm^{-1}, respectively, appeared to be unpolarized. For example, the intensity of AF3 stays constant in both polarization configurations. In addition, it should be noted that in this mid-IR study, the features were not observed in the three

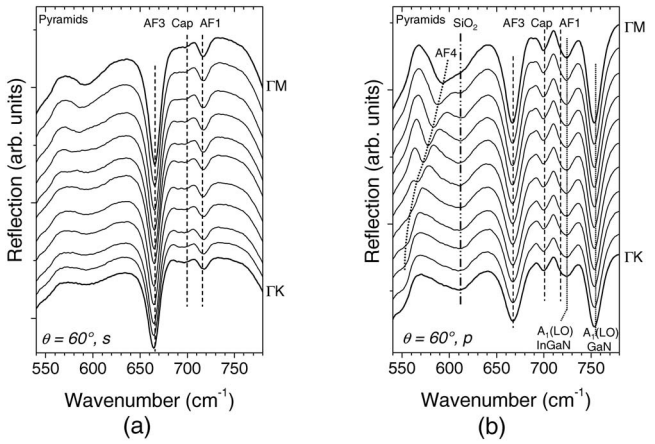

FIG. 8. Typical azimuthal-angle φ dependent reflection spectra showing the dispersion of the features in the mid-IR range. The polarized light is incident at θ=60° and φ is varied from 0° (ΓK direction) to 30° (ΓM direction) in steps of 3°. The lines showing the angular dispersion of the A_1(LO) modes of GaN and $In_xGa_{1-x}N$/GaN SQW and of the additional features are guides to the eye.

planar epilayers representative of component layers in the pyramid arrays. In contrast, the features AF2 and AF4 move significantly with increasing θ.

In order to highlight the different behaviors of the additional features, we also present the *s*- and *p*-reflection spectra taken at an incident angle of 60° and for different values of the azimuthal angle, from φ=0° (ΓK orientation) up to φ =30° (ΓM orientation), in steps of 3° [Figs. 8(a) and 8(b)]. AF1 and AF3 are observed in both *s*- and *p*-polarizations and do not move, whatever the value of φ. Again, AF4 moves significantly with varying φ.

The behavior of the different features as a function of the angle of incidence along the ΓK and ΓM orientations—and as a function of the azimuthal angle for θ=60°—is summarized in Figs. 9(a)–9(c). Four kinds of feature with distinct behavior have been observed: (i) features indicated by dots that blueshift with increasing θ, that do not move with φ and that are not observed in *s*-polarization [A_1(LO) modes of GaN and $In_xGa_{1-x}N$/GaN SQW], (ii) features indicated by open squares and full lines that do not shift, or shift only a little, with θ and φ—and are observed in both polarizations (AF1 and AF3), (iii) features attributed to the cap layer and to the SiO_2 mask layer, which are indicated by solid squares. These features do not shift, or shift only a little, with θ and φ—and are observed more clearly in *p*-polarization; (iv) features indicated by triangles that move significantly with increasing θ and φ (AF2 and AF4). As expected, the A_1(LO) modes of GaN and $In_xGa_{1-x}N$/GaN SQW do not depend on φ [Fig. 9(c)].

We assign the features AF1 ad AF3 to the presence of disorder. More particularly, we assign the feature AF3 at 667 cm^{-1} to disorder activation of the silent B_1(high) mode in agreement with Refs. 25–28. Wieser *et al.*[27] have shown that this mode can become IR-active, and that micro-Raman spectra could provide further indication of disorder (peaks at 667 and 300 cm^{-1}). Disorder is also suggested by our micro-Raman spectra (Fig. 5). In this sense, our micro-Raman spectra with separate excitation at wavelengths of 488 and 647.1 nm probe the sample in different fashions. The Raman spectrum for the 488 nm excitation probes the surface of the pyramids, whereas the excitation at 647.1 nm probes the sample more deeply. A few differences appear when comparing the two spectra. The spectrum for the 488 nm excitation shows no visible defects. In contrast, for the 647.1 nm excitation, we observed the presence of broad bands around 300 cm^{-1}—and in the range of 600–680 cm^{-1}. The Raman band appearing at about 300 cm^{-1} was assigned to disorder or defects in GaN, whereas the band at 667 cm^{-1} in the IR

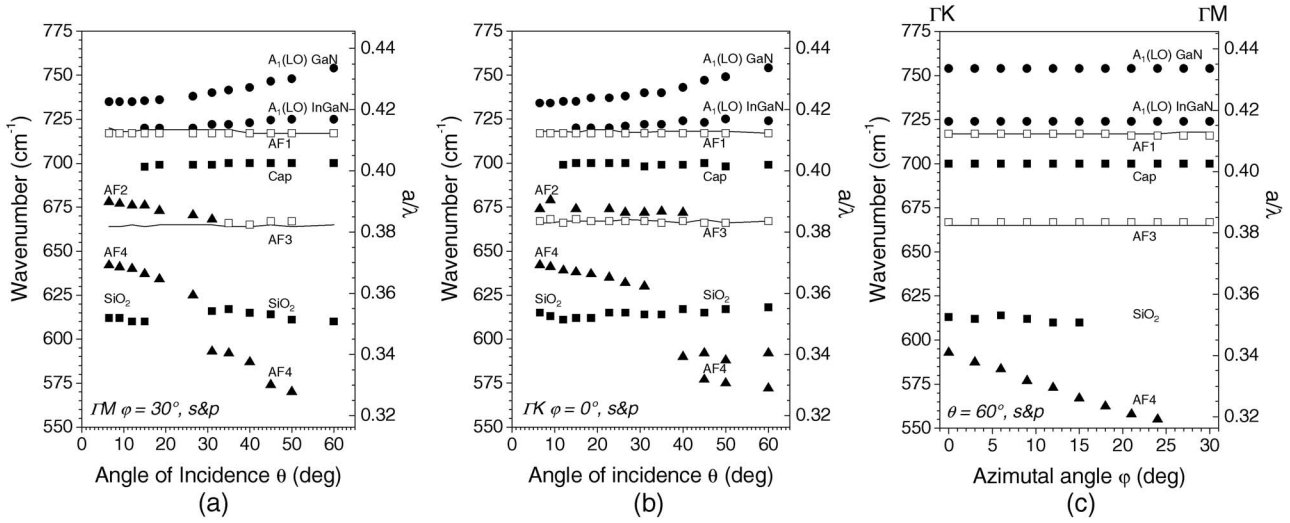

FIG. 9. Position of the features observed in the mid-IR spectra for the selectively grown GaN pyramid array, as a function of the angle of incidence along the ΓM (a) and ΓK (b) symmetry orientations—and as a function of the azimuthal angle at θ=60° (c), for *s*- and *p*-polarizations. Four kinds of feature with distinct behavior have been observed: (●) features that blueshift with increasing θ that do not move with φ and that are not observed in *s*-polarization [A_1(LO) of GaN and $In_xGa_{1-x}N$/GaN SQW]; (—, □) features that do not shift, or shift only a little, with θ and φ and are observed in *s*- and *p*-polarizations, respectively (AF1 and AF3); (■) features attributed to the cap layer and to the SiO_2 mask layer. These features do not shift, or shift only a little, with θ and φ and are observed more clearly in *p*-polarization; (▲) features indicated by triangles and dashed lines that move significantly with increasing θ and φ (AF2 and AF4).

spectra was assigned to disorder activation of the silent B_1 mode due to the presence of damage at the GaN seed layer surface. These observations suggest that some aspect of the processing, possibly ion bombardment during PECVD of the SiO_2 mask layer, introduced lattice disorder in the GaN seed layer beneath the pyramids. AF1 and AF3—and features attributed to the cap layer and to the SiO_2 mask—are not sensitive to the azimuthal angle φ [Fig. 9(c)].

In contrast, the AF4 [observed in Figs. 8(b) and 9(c)] and AF2 (observed for smaller θ) features are sensitive to θ and also to φ. No clear identification can be made for the origin of these features because, to the best of our knowledge, neither IR- nor Raman-active impurity-type modes have been observed to exhibit such optical anisotropy. Such behavior could originate from a cavity effect peculiar to the individual hexagonal microresonators.

V. CONCLUSIONS

In conclusion, SAG on a GaN wurtzite (0001) seed layer partially covered by a patterned SiO_2 mask offers the promise of producing photonic microstructures without using dry etching of the active layers—thus largely avoiding the associated effects of surface damage. Photonic crystal properties have been demonstrated for one of our samples in the near-IR. Surface coupling techniques have been applied to a study of the behavior of structures formed by flat-topped GaN pyramids—and strong photonic crystal characteristics have been observed. The experimental results are in good agreement with the calculated photonic band structure obtained using a scattering matrix formalism. The anisotropic optical properties of the micropyramids in the mid-IR part of the spectrum were also investigated by using *s*- and *p*-polarized reflectance spectra to probe the IR-red active phonons of the array of pyramids. The A_1(LO) phonon of the $In_xGa_{1-x}N/GaN$ SQW was identified and the indium composition was derived from the behavior of the phonon related modes. The additional features observed in the reststrahlen region of GaN, which do not move with changes in the incident and azimuthal angles, are assigned to defects induced in the HT-GaN seed layer possibly by ion bombardment during PECVD of the SiO_2 mask layer. No damage is found to be induced in the active SQW layer(s) grown as a final step. The origin of additional features sensitive to both the incident and azimuthal angles remains unclear. The features could originate from cavity effects peculiar to the individual hexagonal microresonators. An obvious development of this type of structure would be to reduce the size of the pyramids, together with the period of the array—thus providing the ability to influence and control the spontaneous emission processes of embedded quantum wells. Progress toward this latter objective has been reported in Ref. 29.

ACKNOWLEDGMENTS

The authors thank P. Arcade, J. Lyonnet, F. Pichot, M. Ramonda, and J. L. Sauvajol (Université Montpellier 2) for their valuable help with the experiments and W. Knap and J. R. Huntzinger (Université Montpellier 2) for stimulating discussions.

[1] A. Murai, D. B. Thompson, H. Masui, N. Fellows, U. K. Mishra, S. Nakamura, and S. P. DenBaars, Appl. Phys. Lett. **89**, 171116 (2006).
[2] E. H. Park, I. Ferguson, S. K. Jeon, J. S. Park, and T. K. Yoo, Appl. Phys. Lett. **89**, 251106 (2006).
[3] T. N. Oder, J. Shakya, J. Y. Lin, and H. X. Jiang, Appl. Phys. Lett. **83**, 1231 (2003).
[4] H. X. Jiang, J. Y. Lin, K. C. Zeng, and W. Yang, Appl. Phys. Lett. **75**, 763 (1999).
[5] Y.-S. Choi, K. Hennessy, R. Sharma, E. Haberer, Y. Gao, S. P. DenBaars, S. Nakamura, and E. L. Hu, Appl. Phys. Lett. **87**, 243101 (2005).
[6] J. J. Wierer, M. R. Krames, J. E. Epler, N. F. Gardner, M. G. Craford, J. R. Wendt, J. A. Simmons, and M. M. Sigalas, Appl. Phys. Lett. **84**, 3885 (2004).
[7] A. David, C. Meier, R. Sharma, F. S. Diana, S. P. DenBaars, E. Hu, S. Nakamura, C. Weisbuch, and H. Benisty, Appl. Phys. Lett. **87**, 101107 (2005).
[8] S. Fan and J. D. Joannopoulos, Phys. Rev. B **65**, 235112 (2002).
[9] D. Coquillat, S. K. Murad, A. Ribayrol, C. J. M. Smith, R. M. De La Rue, C. D. W. Wilkinson, O. Briot, and R. L. Aulombard, Mater. Sci. Forum **264–268**, 1403 (1998).
[10] J. Torres, D. Coquillat, R. Legros, J. P. Lascaray, F. Teppe, D. Scalbert, D. Peyrade, Y. Chen, M. Le Vassor d'Yerville, E. Centeno, D. Cassagne, and J. P. Albert, Phys. Rev. B **69**, 085105 (2004).
[11] A. Rosenberg, M. W. Carter, J. A. Casey, M. Kim, R. T. Holm, R. L. Henry, C. R. Eddy, V. A. Shamamian, and K. Bussmann, Opt. Express **13**, 6564 (2005).
[12] A. Kasic, M. Schubert, J. Off, B. Kuhn, F. Scholz, S. Einfeldt, T. Bottcher, D. Hommel, D. J. As, U. Kohler, A. Dadgar, A. Krost, Y. Saito, Y. Nanishi, M. R. Correia, S. Pereira, V. Darakchieva, B. Monemar, H. Amano, I. Akasaki, and G. Wagner, Phys. Status Solidi C **0**, 1750 (2003).
[13] R. W. Martin, P. R. Edwards, C. Liu, C. J. Deatcher, H. M. H. Chong, R. M. De La Rue, and I. M. Watson, Inst. Phys. Conf. Ser. **179**, 135 (2003).
[14] H. Mikaye, K. Nakao, and K. Hiramatsu, Superlattices Microstruct. **41**, 341 (2007).
[15] M. Jetter, M. Perez-Solorazano, A. Groening, M. Ubl, H. Graedeldinger, and H. Schweizer, J. Cryst. Growth **272**, 204 (2004).
[16] C. Liu, S. Stepanov, P. A. Shields, A. Gott, W. N. Wang, E. Steimetz, and J.-T. Zettler, Appl. Phys. Lett. **88**, 101103 (2006).
[17] C. J. Deatcher, C. Liu, S. Pereira, M. Lada, A. G. Cullis, Y. J. Sun, O. Brandt, and I. M. Watson, Semicond. Sci. Technol. **18**, 212 (2003).
[18] D. Coquillat, J. Torres, D. Peyrade, Y. Chen, R. Legros, J. P. Lascaray, M. Le Vassor d'Yerville, R. M. De La Rue, E. Centeno, D. Cassagne, and J. P. Albert, Opt. Express **12**, 1097 (2004).
[19] D. M. Whittaker and I. S. Culshaw, Phys. Rev. B **60**, 2610 (1999).
[20] M. Le Vassor d'Yerville, E. Centeno, D. Cassagne, J. P. Albert, Proc. SPIE **5450**, 181 (2004).
[21] U. Haboeck, H. Siegle, A. Hoffmann, and C. Thomsen, Phys. Status Solidi C **0**, 1710 (2003).
[22] S. Hernández, R. Cuscó, D. Pastor, L. Artús, K. P. O'Donnell, R. W. Martin, I. M. Watson, Y. Nanishi, and E. Calleja, J. Appl. Phys. **98**, 013511 (2005).
[23] Z. G. Hu, A. B. Weerasekara, N. Dietz, A. G. U. Perera, M. Strassburg, M. H. Kane, A. Asghar, and I. T. Ferguson, Phys. Rev. B **75**, 205320 (2007).
[24] A. Kasic, M. Schubert, S. Einfeldt, D. Hommel, and T. E. Tiwald, Phys. Rev. B **62**, 7365 (2000).
[25] F. Demangeot, J. Groenen, J. Frandon, M. A. Renucci, O. Briot, S. Ruffenach, and R. L. Aulombard, Appl. Phys. Lett. **72**, 2674 (1998).
[26] F. Demangeot, J. Gleize, J. Frandon, M. A. Renucci, M. Kuball, D. Peyrade, L. Manin-Ferlazzo, Y. Chen, and N. Grandjean, J. Appl. Phys. **91**, 2866 (2002).
[27] N. Wieser, O. Ambacher, H. Angerer, R. Dimitrov, M. Stutzmann, B. Stritzker, and J. K. N. Lindner, Phys. Status Solidi B **216**, 807 (1999).
[28] M. H. Kane, M. Strassburg, A. Asghar, W. E. Fenwick, J. Senawiratne, Q. Song, C. J. Summers, Z. J. Zhang, N. Dietz, and I. T. Ferguson, Mater. Sci. Eng., B **126**, 230 (2006).
[29] D. Coquillat, M. Le Vassor d'Yerville, S. A. Boubanga Tombet, C. Liu, K. Bejtka, I. M. Watson, P. R. Edwards, R. W. Martin, H. M. H. Chong, and R. M. De La Rue, Phys. Status Solidi C **4**, 99 (2007).